第 48 卷第 12 期
2020 年 12 月

硅 酸 盐 学 报
JOURNAL OF THE CHINESE CERAMIC SOCIETY

Vol. 48，No. 12
December，2020

http://www.gxyb.cbpt.cnki.net

DOI：10.14062/j.issn.0454-5648.20200333

成型压力对微波烧结的复杂 Ti(C, N)基金属陶瓷刀具力学性能和显微结构的影响

殷增斌，叶佳冬，朱智勇，洪东波

(南京理工大学机械工程学院，南京 210094)

摘　要：采用微波烧结技术制备了复杂刃形 Ti(C, N)基金属陶瓷刀具，利用仿真和实验的方法研究了压制压力对复杂 Ti(C, N)基金属陶瓷刀具素坯密度分布均匀性、残余应力，以及素坯烧结后刀具前/后刀面致密度、力学性能和微观组织的影响。结果表明：模压成型和微波烧结相结合的技术可制备高性能复杂陶瓷刀具；刃口区域的密度值小于非刃口区域的密度值，其差值随着压制压力的提高先增大后减小。当压制压力≤200 MPa 时，前后刀面的相对密度和力学性能相差不大；压制压力≥300 MPa 时，前刀面的相对密度和力学性能均优于后刀面，但过高的压制压力会导致刀具内部产生裂纹；三维槽型 Ti(C, N)基金属陶瓷刀具的最佳压制压力为 400 MPa。

关键词：微波烧结；碳氮化钛陶瓷；压制压力；显微结构；力学性能
中图分类号：TB332　**文献标志码**：A　**文章编号**：0454–5648(2020)12–1906–08
网络出版时间：2020–10–13



Effects of Molding Pressure on Mechanical Properties and Microstructure of Microwave Sintered Complex-shaped Ti(C, N) Cermet Tool

YIN Zengbin, *YE Jiadong*, *ZHU Zhiyong*, *HONG Dongbo*
(School of Mechanical Engineering, Nanjing University of Science and Technology, Nanjing 210094, China)

Abstract: A complex-shaped titanium carbonitride (Ti(C, N))-based cermet tool was prepared by microwave sintering. The effects of molding pressure on density distribution and residual stress of green compact, relative density, mechanical properties, and microstructure of the sintered compact tool were studied. The results indicated that a high-performance complex-shaped ceramic tool can be prepared using the combined technology of molding and microwave sintering. The density of the cutting edge was lower than that of the body of the tool. The difference increased first and then decreased with the increase in molding pressure. When the molding pressure was lower than 200 MPa, minimal differences between rake and flank faces with respect to relative density and mechanical properties were noted, while the relative density and mechanical properties of rake face were higher than that of flank face when the molding pressure was higher than 300 MPa. However, excessive molding pressure resulted in cracks within the tool. The optimal molding pressure for preparation of a Ti(C, N)-based cermet tool with three-dimensional breaker was 400 MPa.

Keywords: microwave sintering, titanium carbonitride ceramic, molding pressure, microstructure, mechanical property

1 Introduction

Titanium carbonitride (Ti(C, N))-based cermet tool has great advantages in the fields of high-speed cutting and the machining of difficult-to-cut materials owing to its excellent abrasion good heat resistances and chemical stability. Although its hardness is a little lower than that of ceramic tools made of aluminum oxide (Al_2O_3) or titanium diboride (TiB_2), it possesses

收稿日期：2020–05–11。　修订日期：2020–06–03。
基金项目：国家自然科学基金(51875291)；江苏省优秀青年基金(BK20190070)；江苏省“六大人才高峰”高层次人才计划(GDZB-016)和中央高校基本科研业务费专项资金(30920032206)资助。
第一作者：殷增斌(1987—)，男，博士，副教授。

Received date: 2020–05–11.　**Revised date:** 2020–06–03.
First author: YIN Zengbin (1987–), male, Ph.D., associate Professor.
E-mail: zengbinyin@njust.edu.cn

preferable flexural strength and fracture toughness. Therefore, Ti(C, N) is commonly used in the machining of alloys and stainless steels[1–4].

Modern high efficiency, high precision, highly reliable, and specialized cutting tools are undergoing development. In addition, complex tool structures are also being developed. Tool edges are changing from linear to spiral and waved edges, and tools are equipped with either two- or three-dimensional (2/3D) chip breakers. The complex tool structures are beneficial not only to the machining of complex-shaped parts, but slow down tool wear and improve processing efficiency.

Now, Ti(C, N)-based cermet tools are commonly prepared by pressureless sintering(PS), hot-pressing sintering (HP), hot isostatic pressing sintering (HIP), and spark plasma sintering (SPS)[5–20]. However, HP, HIP, and SPS can only be used to prepare simple-shaped ceramic tools (tools with flat rake faces and linear cutting edges) on account of the pressure process during sintering. Although the complex-shaped ceramic tool can be prepared by pressureless sintering, the mechanical properties and microstructure of ceramic tools have difficulties meeting the requirements of high-speed machining owing to the high sintering temperatures, long sintering periods, and uneven temperature fields in traditional pressureless sintering.

Microwave sintering is a novel pressureless sintering, whose sintering mechanisms are essentially different from the traditional pressureless sintering. For microwave sintering, heat is generated by the coupling interaction between electromagnetic field and material, which is different from the radiation heat transfer of traditional sintering, so the whole sample is heated rapidly and evenly, and there is no temperature gradient within the sample[21–22]. Furthermore, the use of the microwave could decrease the sintering activation energy and accelerate mass transfer of ceramic materials, which is called microwave effects[23–25]. In recent years, microwave sintering had been used in the preparation of ceramics, such as Al_2O_3, silicon nitride (Si_3N_4), TiB_2, Ti(C, N), zirconium oxide (ZrO_2), and cemented carbides[26–31], which possess fine microstructure and high levels of mechanical property characteristics. Therefore, due to the characteristics of pressureless sintering and microwave-related effects, microwave sintering shows great potential for integrated preparation of ceramic tools with complex structures and high mechanical properties.

Raw property materials, molding technologies, and sintering process are vital to microwave-sintered ceramics. No pressure is applied to the sample in microwave sintering; thus, the performances of green compact tools, especially their density distributions, have great effects on the mechanical properties of such tools. For the die-pressed compact prepared using single-ended uniaxial molding, uniaxial pressure plays an important role in the density and microstructure of green compact machines and tools. The defects in green compact tools due to improper modeling would lead to a sharp degradation in mechanical properties of these tools[32]. However, studies on the preparation of complex-shaped ceramic tools using microwave sintering and effects of molding pressure effects on densification, microstructure, and mechanical properties of microwave sintered ceramics have rarely been reported.

In this study, Ti(C, N)-based ceramic tools with three-dimensional (3D) chip breakers were prepared by microwave sintering. Distribution of density and residual stress within the green tool samples were studied by simulation. Effects of molding pressure on relative density, mechanical properties, and microstructures of rake and flank faces of ceramic tool were studied.

2 Experimental

The cermet tool was composed of Ti(C, N) (mass ratio C:N=7:3), tungsten carbide (WC), molybdenum carbide (Mo_2C), Mo, Ni, and cobalt (Co), and details of the raw powders can be found in[33]. The mixed powders were ball-milled for 24 h, and then dried at 120 ℃ under a vacuum. After that, the dried powders were sieved through a 100 mesh sieve (mesh aperture 0.15 mm). The green tool body was formed in a mold with the application of axial pressure of 100~500 MPa for 2 min. Finally, the green tool was sintered at 1 600 ℃ for 20 min in flowing N_2 atmosphere in a 2.45 GHz multimode microwave furnace.

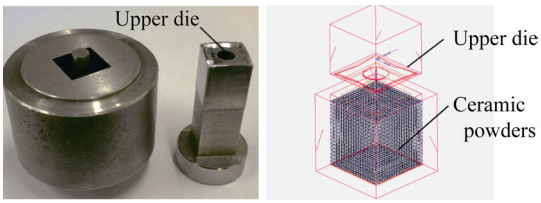
The relative density was measured by Archimedes' method. Vickers hardness was measured with a hardness tester with load of 196 N and holding time of 15 second. Fracture toughness was obtained by the Vickers indentation method[34]. The relative density, Vickers hardness, and fracture toughness were tested five times, and the average values were calculated. Fractured surfaces were observed by scanning electron microscopy (SEM) equipped with energy-dispersive X-ray spectroscopy (EDS) from SEM, FEI Quanta 250F.

3 Results and discussion

3.1 Density distribution of green ceramic tool during compaction

Finite-element simulation was applied to investigate the density distribution of green ceramic tool in the process of compaction. In order to ensure higher relative density of the cutting edge, the chip breaker was made on the upper die as shown in Fig. 1(a). The simulation of compaction of powders was conducted by the software of MSC. Marc. The

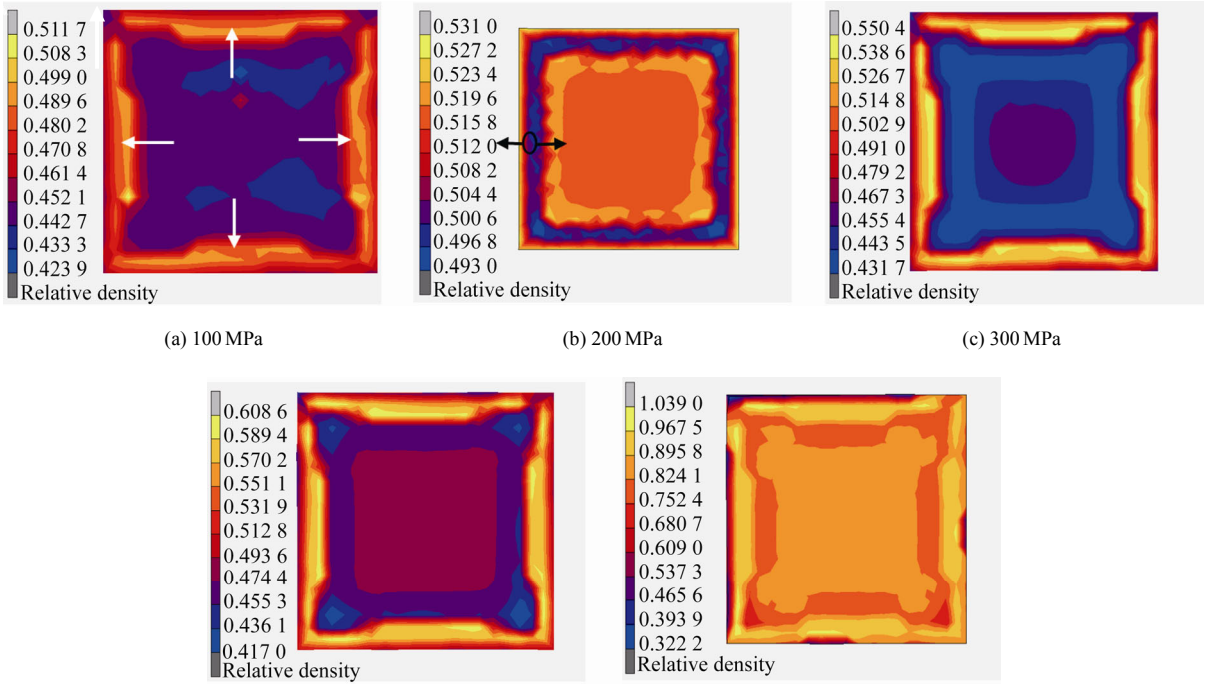
numerical simulation model is given in Fig. 1(b). The length and width of the numerical simulation model were 13 mm, and the initial loose-fitting height was 20 mm. The four-node quadrilateral element was adopted in the mesh division of the simulation process. Three-hundred ninety-six layers of elements in the direction of side length, 20 layers of elements in the direction of height, and a total of 7920 elements were used. The elastic modulus E and Poisson's ratio ν of simulated material are defined as $E=E_0\ \rho^{3.6}$[35] and $\nu=0.5e^{-12.5(1-\rho)\wedge 2}$[36], respectively, in which E_0 is the elastic modulus of the dense Ti(C, N) ceramic tool (460 GPa), and ρ is the relative density. The Shima-Oyane material constitutive model was adopted for the yield criterion. The frictional coefficient between the ceramic powders and mold was approximately equal to 0.1, so Coulomb's law of friction was adopted[37].



(a) Die (b) Simulation model

Fig. 1 Die and simulation model

The density distribution of the green ceramic tool after compaction at pressures of 100 to 500 MPa (in 100 MPa increments) was studied. As can be seen in Fig. 2, with an increase in compaction pressure, relative density of the green compact tool increased and the density gradient became lower. When the pressure was 100 MPa, the areas near the cutting edge and chip breaker (indicated by the arrows) possessed the highest density (Fig. 1(a)). This process occurred because the ceramic powders first came into contact with the cutting edge and chip breaker of the upper die. Thus, the ceramic powders had a longer time to flow to reduce gaps among the particles. When the pressure was increased to 200 MPa, the smallest density of the green compact tool appeared in the groove, but densities of the areas around the groove distributed circularly and were higher than those of the groove as shown in Fig. 2(b). The groove on the upper die was a slope, so the particles would have flowed horizontally with the application of pressure as indicated by the arrows in Fig. 2(b). Therefore, the density around the groove increased because the gaps were filled with flowing particles. When the pressure increased to 300 MPa, the density gradient became much larger than that at 200 MPa, whereas the areas near the cutting edge achieved the highest density once again (Fig. 2(c)). This phenomenon might have been due to inhibition of particle flow in the final stage of compaction under high pressure of 300 MPa since the shear force between powder particles was also enhanced[38]. In this instance, densification was more related to the elastic-plastic deformation of powders, which was directly determined by the pressure[39]. Due to the groove slope, the downward force was much larger than the force that was perpendicular to the



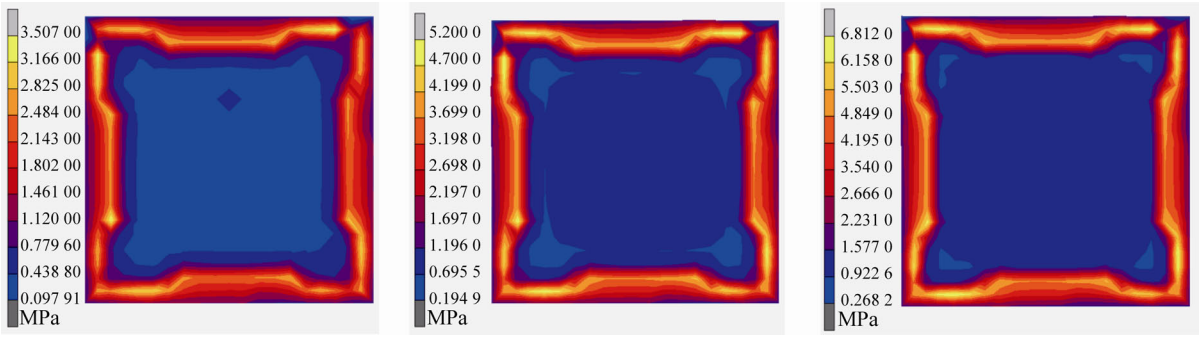
(a) 100 MPa (b) 200 MPa (c) 300 MPa

(d) 400 MPa (e) 500 MPa

Fig. 2 Density distribution of green ceramic tools when compacted at different pressures

slope. Thus, the highest density appeared at the cutting edge, whereas the lowest density was at the top of the chip breaker. When the pressure increased to higher levels of 400 and 500 MPa, particle flow inhibition was maintained, and the density distribution of the green compact tool was similar to at of 300 MPa. Higher pressure led to larger elastic-plastic deformation and also higher density. The density of the green compact tool that was compacted at 500 MPa was the highest, and the density gradient was the smallest.

Residual stress within the green tools after compaction was also investigated by MSC. Marc software system. Figs. 3(a)–3(c) shows the residual stress distribution in the green tools compacted at pressures of 100, 300, and 500 MPa. The residual stress increased with the increase in pressure. The residual stress was unevenly distributed, and the areas with higher density had higher residual stress. Greater elastic-plastic deformation in these areas lead to more energy was stored there. Non-uniformity of the residual stress became more severe with the increase in compaction pressure.



(a) 100 MPa　　(b) 300 MPa　　(c) 500 MPa

Fig. 3　Residual stress within green tools after compacted at different pressures

3.2　Mechanical property

The image of the complex-shaped tool prepared by microwave sintering is shown in Fig. 4. The relative density, Vickers hardness and fracture toughness of rake face and flank face of the tool after microwave sintering are given in Fig. 5.

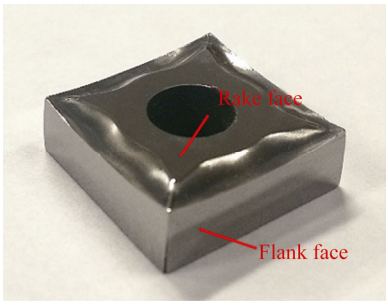


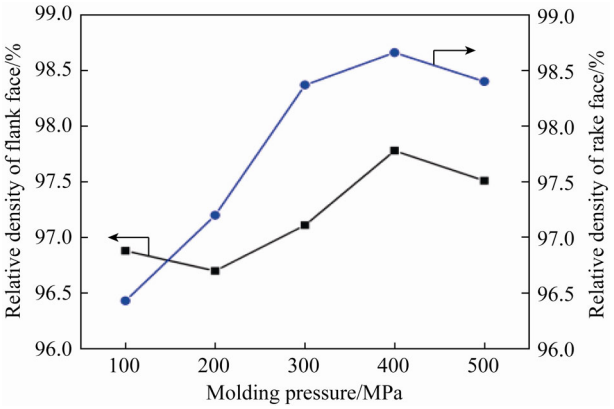
Fig. 4　Optical picture of the tool after microwave sintering

Relative densities of both the rake and flank faces increased as the molding pressure increased from 100 to 400 MPa, but the density of the rake face was higher than that of flank face as shown in Fig. 5(a). This finding was consistent with the density distribution of the green samples (Fig. 2). Due to the axial pressure applied during compaction of green tools, the density of the rake face of the green tool was higher than the flank face. Hardness and toughness of rake face were higher than that of flank face at each molding pressure, and the difference between rake and flank faces became lager with the increase in molding pressure (Fig. 5(b) and (c)). This variation trend was also attributed to the different densities of the flank and rake faces of the green tool. Generally, higher density results in better mechanical properties.

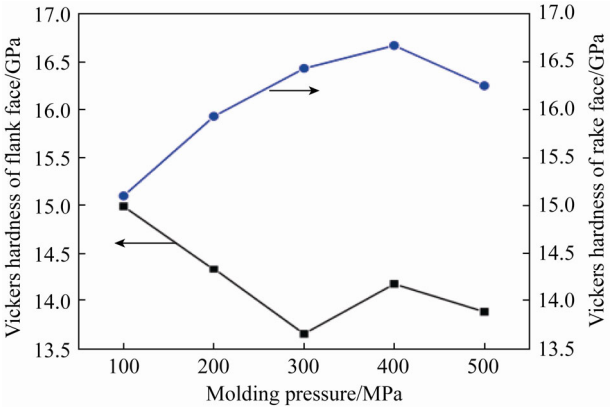
It was worth noting that relative density and hardness of both the rake and flank faces decreased when the molding pressure was increased to 500 MPa. Defects, such as layering, cracks, and holes were observed in the sintered tool (Fig. 6) when the molding pressure was 500 MPa. As an axial pressure was applied to the green compact tool, the density and residual stress within the green compact tool decreased from top to bottom and became distributed in layers[40–41]. During the molding process, the height of the green compact decreased with the increase in molding pressure; thus, a greater amount of elastic deformation energy would be stored within the body. The stored energy could be released in the de-molding process. Thus, when the green tool was ejected from the die, the internal defects (Fig. 6) would be produced by the elastic-after-effect. This process could have caused degradation of mechanical properties of the sintered tool.

3.3　Microstructure

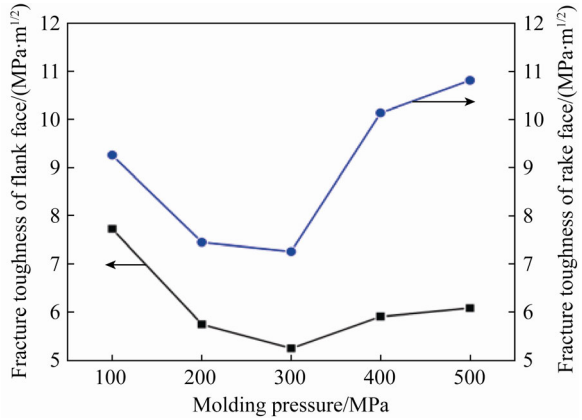
The microstructure of the areas near the rake and flank faces (indicated in Fig. 7) were studied. SEM micrographs of fractured surface near the flank face of the tool compacted at different pressures are shown in Fig. 8. When the molding pressures were 100 and



(a)Relative density



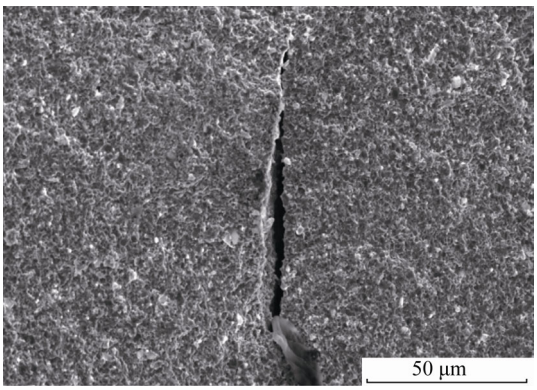
(b) Vickers hardness



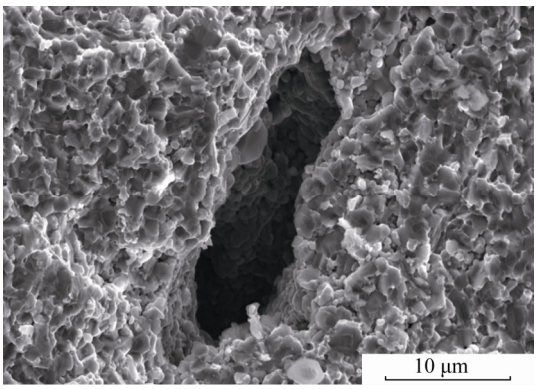
(c) Fracture toughness

Fig. 5 Mechanical properties of rake face and flank face of the tool compacted at different molding pressure

200 MPa, densification was poor, and numerous pores within the body existed as indicated by the arrows in Fig. 8a and b. As the molding pressure increased to 300 and 400 MPa, the microstructure became homogeneous, the grains contacted tightly, and the pores disappeared (Fig. 8(c) and (d)). Moreover, trans-crystalline and inter-crystalline fractures coexisted, which benefited the enhancement of the mechanical properties of the ceramic materials. When the molding pressure was 500 MPa, cracks existed in the body as shown in Fig. 8(e) although no pore existed. The cracks were induced by the high gradient residual stress as discussed in section 3.2.



(a) Crack



(b) Hole

Fig. 6 SEM micrograph of fractured surface of the sintered tool when the molding pressure was 500 MPa

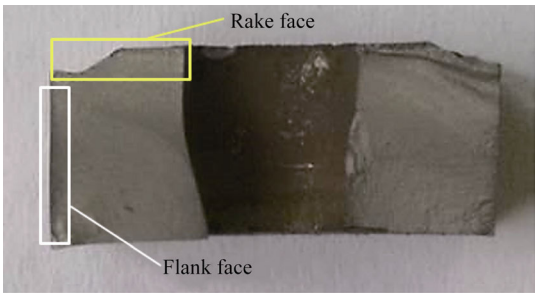
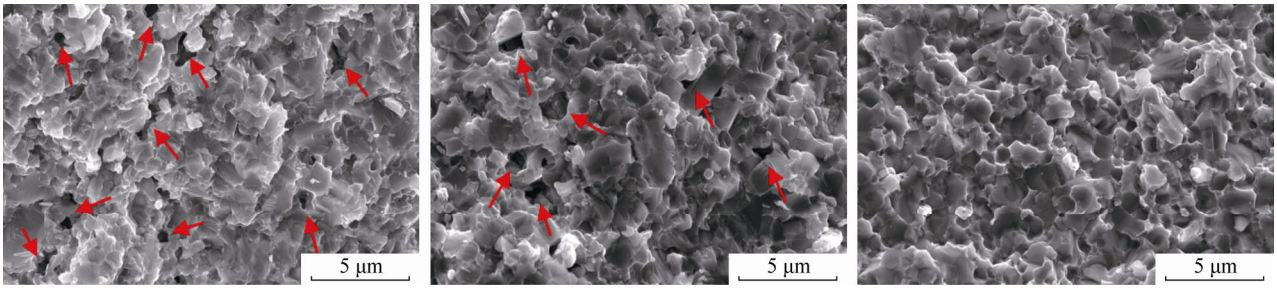


Fig. 7 Optical picture of fractured surface of sintered tool

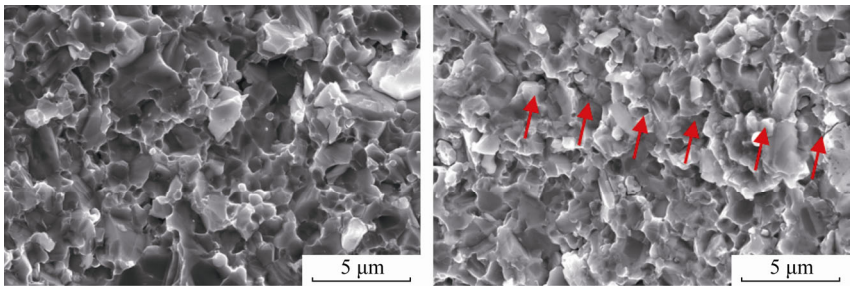
Fig. 9 shows the SEM micrograph of fractured surface near the flank face of the tool that was compacted under different pressures. When the molding pressure was 100 MPa, the flank face had poor densification, and some particles (indicated by the arrows) were still in powder morphology. The grains were loosely contacted, and a lack of metallic bonded phases among the grains as indicated by the dotted box in Fig. 9(a) could be observed. As the molding pressures increased to 200 and 300 MPa, the

microstructure became dense, but some pores still remained as shown in Figs. 9(b) and 9(c). When the molding pressures were 400 and 500 MPa as shown in Fig. 9(d) and 9(e), the microstructure was homogeneous, and the grains were arranged tightly. It was worth noting that with the increase in molding pressure, the grains were bonded with more binder phases, especially at 500 MPa as indicated by the dotted box in Figs. 9(d) and 9(e).

An EDS analysis was done, and the result was shown in Fig. 10. As can be seen from Fig. 10(a) and (b), the binder phases (area *A* in Fig.10(a)) were mainly the metallic phases of Ni, Mo, and Co. Thus, it could be concluded that more metallic phase content aggregated around the flank face with the increase in molding pressure. To some extent, this increase contributed to densification of the flank face.

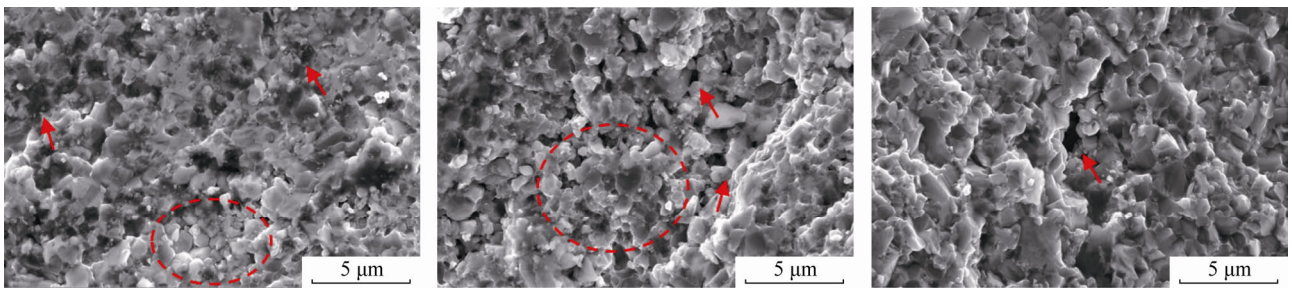


(a) 100 MPa　　(b) 200 MPa　　(c) 300 MPa

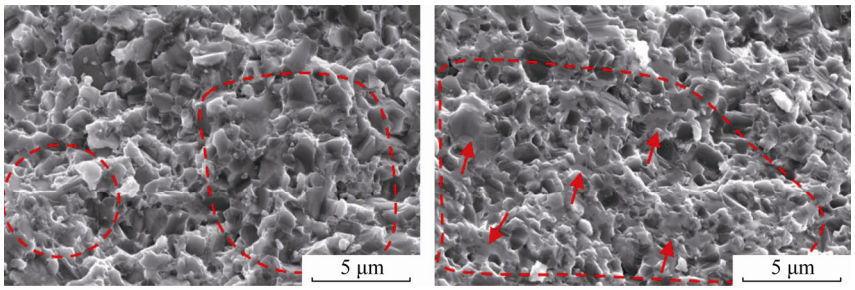


(d) 400 MPa　　(e) 500 MPa

Fig. 8　SEM micrograph of fractured surface near rake face of the tool compacted at different pressures

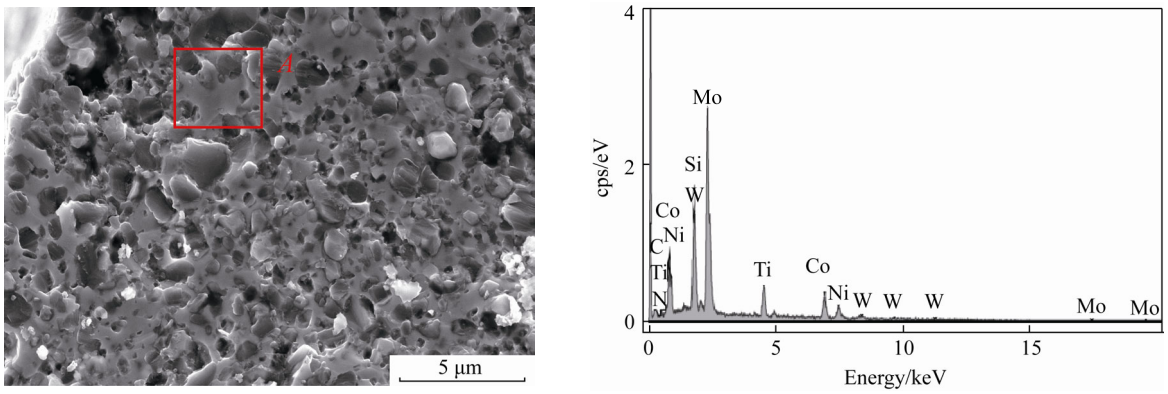


(a) 100 MPa　　(b) 200 MPa　　(c) 300 MPa



(d) 400 MPa　　(e) 500 MPa

Fig. 9　SEM micrograph of fractured surface near flank face of the tool compacted at different pressures



(a) SEM micrograph of flank face (b) EDS spectrum of areas *A*

Fig. 10 SEM micrograph of flank face compacted at 500MPa and EDS spectrum of areas *A*

4 Conclusions

1) The complex-shaped Ti(C, N)-based ceramic tool with satisfactory mechanical properties can be prepared via microwave sintering. The density of the green tool increased with the increase in molding pressure, but the density of the cutting edge was lower than that of the tool body, and the difference first increased followed by a decrease as the molding pressure increased.

2) The mechanical properties of the rake face were higher than that of the flank face. The mechanical property difference between the rake and flank faces became lager as the molding pressure increased to 300 MPa due to the different densities of the flank and rake faces in the molding process of the green tool. The optimal mechanical properties of both the rake and flank faces were optimal when the molding pressure was 400 MPa.

3) The microstructure of the sintered tool became homogeneous, and the grains were in tight contact as the molding pressure increased. Cracks and holes were produced due to the release of residual stress when the molding pressure reached 500 MPa.

References:

[1] MUHAMMAD R, AHMED N, ROY A, et al. Turning of advanced alloys with vibrating cutting tool[J]. Solid State Phenom, 2012, 18(1): 277–284.

[2] WANG Y, ZOU B, WANG J, et al. Effect of the progressive tool wear on surface topography and chip formation in micro-milling of Ti-6Al-4V using Ti(C7N3)-based cermet micro-mill[J]. Tribol Int, 2019, 141(1): 1–14.

[3] MANOJ KUMAR B V, RAM KUMAR J, BIKRAMJIT B. Crater wear mechanisms of Ti(C, N)-Ni-WC cermets during dry machining[J]. Int J Refract Met Hard Mater, 2007, 25(2): 392–399.

[4] KUMAR C S, MAJUMDER H, KHAN A, et al. Applicability of DLC and WC/C low friction coatings on Al_2O_3/TiCN mixed ceramic cutting tools for dry machining of hardened 52100 steel[J]. Ceram Int, 2020, 46(8, Part B): 11889–11897.

[5] XIONG H, WEN Y, GAN X, et al. Influence of coarse TiCN content on the morphology and mechanical properties of ultrafine TiCN-based cermets[J]. Mater Sci Eng A, 2017, 682: 648–655.

[6] ZENG W, GAN X, LI Z, et al. Effect of WC addition on the microstructure and mechanical properties of TiN-based cermets[J]. Ceram Int, 2017, 43(1): 167–173.

[7] XIONG H, LI Z, ZHOU K. TiC whisker reinforced ultra-fine TiC-based cermets: microstructure and mechanical properties[J]. Ceram Int, 2016, 42(6): 6858–6867.

[8] LIU A, LIU N. Effect of WC–Co granules on mechanical properties and microstructure of Ti(C, N)-based cermets[J]. Ceram Int, 2016, 42(14): 15274–15284.

[9] AKINRIBIDE O J, OBADELE B A, AKINWAMIDE S O, et al. Sintering of binderless TiN and TiCN-based cermet for toughness applications: Processing techniques and mechanical properties: A review[J]. Ceram Int, 2019, 45(17, Part A): 21077–21090.

[10] MERWIN XAVIER A M D, NEEVATHA S B, SWATHI SELVI S, et al. Wear and thermal stability of nano-TiB_2 modified TiCN–WC–Co–Cr_3C_2 cermet[J]. Int J Refract Met Hard Mater, 2020, 86(2): 105–130.

[11] SHANKAR E, BALASIVAN S, PRABU H, et al. Mechanical properties and microstructures of TiCN/nano-TiB_2/TiN cermets prepared by spark plasma sintering[J]. Ceram Int, 2018, 44(8): 9384–9394.

[12] CHEN M, ZHUANG Q, LIN N, et al. Improvement in microstructure and mechanical properties of Ti(C, N)-Fe cermets with the carbon additions[J]. J Alloy Comp, 2017, 701: 408–415.

[13] LIU G, LI R, YUAN T, et al. Spark plasma sintering of pure TiCN: Densification mechanism, grain growth and mechanical properties[J]. Int J Refract Met Hard Mater, 2017, 66: 68–75.

[14] WAN W, XIONG J, LIANG M. Effects of secondary carbides on the microstructure, mechanical properties and erosive wear of Ti(C, N)-based cermets[J]. Ceram Int, 2017, 43(1, Part B): 944–952.

[15] SHANKAR E, BALASIVAN S, PRABU H. Influence of WC and cobalt additions on the microstructural and mechanical properties of TiCN-Cr_3C_2-nano-TiB_2 cermets fabricated by spark plasma sintering[J]. Int J Refract Met Hard Mater, 2017, 69: 110–118.

[16] SHANKAR E, Balasivan S, Prabu H. Microstructure and mechanical properties of Ti(C, N) based cermets reinforced with different ceramic particles processed by spark plasma sintering[J]. Ceram Int, 2017, 43(14): 10817–10823.

[17] ZHOU H, HUANG C, ZOU B. Effects of metal phases and carbides on the microstructure and mechanical properties of Ti(C, N)-based cermets cutting tool materials[J]. Mater Sci Eng A, 2014, 618: 462–470.

[18] RAFIAEIA S, BAHRAMIB A, SHOKOUHIMEHR M. Influence of Ni/Co binders and Mo_2C on the microstructure evolution and mechanical properties of $(Ti_{0.93}W_{0.07})C$-based cermet[J]. Ceram Int, 2018, 44(10): 17655–17659.

[19] ZHOU W, ZHENG Y, ZHAO Y, et al. Microstructure characterization and mechanical properties of Ti(C, N)-based cermets with AlN addition[J]. Ceram Int, 2015, 41(3): 5010–5016.

[20] CHOONGKWON P, SANGWOO N, SHINHOO K. Enhanced toughness of titanium carbonitride-based cermets by addition of (Ti, W)C carbides[J]. Mater Sci Eng A, 2016, 649: 400–406.

[21] CHIRAG S, QASIM M, PARVEJ. Microwave Sintering of Advanced Composites Materials: A Review[J]. Mater Today: Proceed, 2018, 5(11, Part 3): 24287–24298.

[22] RAMESH S, ZULKIFLI N, TAN C Y, et al. Comparison between microwave and conventional sintering on the properties and microstructural evolution of tetragonal zirconia[J]. Ceram Int, 2018, 44(8): 8922–8927.

[23] SUN H, ZHANG Y, GONG H T, et al. Microwave sintering and kinetic analysis of Y_2O_3-MgO composites[J]. Ceram Int, 2014, 40(7, Part B): 10211–10215.

[24] YIN Z, YUAN J, CHENG Y, et al. Microstructure evolution and densification kinetics of Al_2O_3/Ti(C, N) ceramic tool material by microwave sintering[J]. Int J Refract Met Hard Mater, 2016, 61: 225–229.

[25] ZUO F, SAUNIER S, MARINEL S, et al. Investigation of the mechanism(s) controlling microwave sintering of α-alumina: Influence of the powder parameters on the grain growth, thermodynamics and densification kinetics[J]. J Eur Ceram Soc, 2015, 35(3): 959–970.

[26] HONG D, YIN Z, YAN S, et al. Fine grained Al_2O_3/SiC composite ceramic tool material prepared by two-step microwave sintering[J]. Ceram Int, 2019, 45(2): 11826–11832.

[27] YIN Z, XU W, YUAN J, et al. Effect of metal phases on microstructure and mechanical properties of Si_3N_4-based ceramic tool materials by microwave sintering[J]. Ceram Int, 2018, 44(16): 19872–19878.

[28] RAMESH S, ZULKIFLI N, TAN C Y, et al. Comparison between microwave and conventional sintering on the properties and microstructural evolution of tetragonal zirconia[J]. Ceram Int, 2018, 44(8): 8922–8927.

[29] MANSHOR H, EZZAT C A, AHMAD Z A, et al. Microwave sintering of zirconia-toughened alumina (ZTA)-TiO_2-Cr_2O_3 ceramic composite: The effects on microstructure and properties[J]. J Alloy Comp, 2017, 722(1): 458–466.

[30] DEMIRSKYI D, CHENG J, AGRAWAL D, et al. Densification and grain growth during microwave sintering of titanium diboride[J]. Scripta Mater, 2013, 69(8): 610–613.

[31] BAO R, YI J, PENG Y, et al. ZHANG. Effects of microwave sintering temperature and soaking time on microstructure of WC-8Co[J]. Trans Nonferrous Met Soc China, 2013, 23(2): 372–376.

[32] ZHANG C, LIU Q B, Present status and prospect of preparation of Ti(C,N)-based cermets[J]. Chin Ceram, 2012, 9(1): 1–4.

[33] YE J, YIN Z, YUAN J, et al. Effects of metal phases on microstructure and mechanical properties of microwave-sintered Ti(C, N)-based cermet tool[J]. Int J Appl Ceram Tech, 2019, 17: 761–770.

[34] EVANS A, CHARLES E. Fracture toughness determinations by indentation[J]. J Am Ceram Soc, 1976, 59: 371–372.

[35] WAGH A S, POEPPEL R B, SINGH J P. Open pore description of mechanical properties of ceramics[J]. J Mater Sci, 1991, 26(2): 3862–3868.

[36] REN Xueping. Study on yield criterion and flow stress of powder metal (in Chinese, dissertation). Harbin: Harbin Institute of Technology, 1989.

[37] WANG DG, WU Y C, JIAO MH, et al. Finite element simulation of influence of different compacting processes on powder metallurgic products properties[J]. Chin J Mech Eng, 2008, 44: 205–211.

[38] MONTILHA F S, ROCCO F O, MELO C C, et al. Identification of dilatancy in green compacted ceramic powder via digital image correlation[J]. Powder Technology, 2018, 330: 471–476.

[39] STUPKIEWICZ S, PICCOLROAZ A, BIGONI D. Elastoplastic coupling to model cold ceramic powder compaction[J]. J Eur Ceram Soc, 2014, 34(11): 2839–2848.

[40] YIN Z, YE J, HONG D, et al, Effect of molding pressure on structural and densification behavior of microwave sintered ceramic tool material[J]. Int J Appl Ceram Tech, 2019, 1(1): 1–9.

[41] ÖZKAN N, BRISCOE B J. Characterization of die-pressed green compacts[J]. J Eur Ceram Soc, 1997, 17(5): 697–711.